

Automatic Identification of Local Geometric Properties During Teleoperation

Thomas Debus and Pierre Dupont

Aerospace and Mechanical Engineering
Boston University
Boston, MA 02215

Robert Howe

Division of Engineering and Applied Sciences
Harvard University
Cambridge, MA 02138

Abstract

During teleoperation, a human operator often receives only 2-D visual feedback from the remote environment. While a variety of kinematic sensors exist on the remote manipulator for control purposes, the information inherent in these signals is rarely extracted and presented to the operator in a useful form. This paper investigates the extraction of such information through the development of an algorithm that estimates the geometric properties of a manipulated object and its environment using the remote robot's sensors and knowledge of the task being performed. The focus of the paper is the development of contact constraint equations parameterized by the desired geometric properties and the automatic segmentation of the data stream according to the set of active contacts. The approach is validated for three-dimensional peg-in-hole insertion using a desktop teleoperator system.

1. Introduction

In many applications, the concept of providing task specific feedback to the operator during teleoperation is an appealing one, which could both improve the system's performance and its safety. As an example, consider an undersea teleoperation task where the goal is to insert a hydraulic connector into a tight socket. Limited visual feedback renders the timely completion of this task difficult. One solution is to use the data collected during the task to automatically build geometric models of the connector and socket and to use these models to guide the operator to task completion. Additional applications in unstructured environments include interplanetary exploration, toxic waste remediation [8] and explosive defusing.

In this paper, we investigate the use of kinematic measurements collected during object manipulation to estimate the geometric properties of those objects. This work builds on our previous results published in [3] and

extends them to three dimensions. Contact states are described using constraint equations parameterized by the geometric properties that we wish to identify.

The paper is laid out as follows. The next section reviews the framework for automatic property estimation first presented in [4]. The following section describes how contact states of 3D objects can be described using sets of parameterized constraint equations. Multiple model estimation based on least squares and correlation coefficients is presented as a means to segment the data stream according to the active contacts. The subsequent section describes an experimental evaluation of this approach using a desktop teleoperator system. A three dimensional peg-in-hole insertion is carried out and the geometrical properties of the peg and hole are estimated. Conclusions are presented in the final section of the paper.

2. Solution Procedure and Background

To solve the automatic property estimation problem, we employ the solution framework described in [4]. The overall problem can be solved as a sequence of three interrelated subproblems: task decomposition, data segmentation and property estimation. These three subproblems are formally described in [4] and can be summarized as follows:

1. Task decomposition - The process of resolving a task into a minimal sequence of *subtasks* described by contact states and their associated properties.
2. Data segmentation - Given a task decomposition and the sensor data stream, find the time intervals corresponding to each subtask.
3. Property estimation - Given the time intervals associated with each subtask, estimate the desired properties.

2.1 Prior Work

The automatic modeling of remote environments has received limited attention in the literature. The three

individual subproblems, however, have been studied in other contexts. Since this paper focuses on data segmentation and property estimation, only these two subproblems are discussed here.

For the purpose of segmentation, a variety of modeling approaches has been employed. The most common methods include hidden Markov models [9], generalized likelihood ratio tests [5], qualitative reasoning with thresholding [11], neural networks for off-line segmentation [6] and Petri nets [12].

Most work on property estimation assumes a parameterized model, e.g., a geometric or contact force model, is given. A significant portion of this literature is devoted to robot parameter estimation. Methods for estimating payload inertia appear in the work of Lin and Yae [10]. Lin and Yae also estimate certain parameters relating to constraints of the operating environment.

To model the properties of objects during manipulation, a central issue is the question of how to model the contact states. A considerable literature on this topic appears in the context of grasping. For example, a kinematic description of two bodies undergoing point contact is studied in the work of Cai and Roth [2], utilizing kinematic and tactile sensing. Other related works include that of Bruyninckx et al who estimate local geometric properties using active force sensing together with kinematic and geometric descriptions of the contact states [1].

In this paper, we assume that the following are given:

- A network of contact states describing allowable state transitions during a task.
- A list of geometric properties to be estimated.

The goals of the paper are to provide the following:

- A standard formulation for expressing a contact state's kinematic constraints.
- A means of generating a sufficient number of contact state constraint equations to solve for the desired properties.
- A simple multiple model approach to data segmentation and estimation.

These topics are described in the sections below.

3. Contact Constraints Segmentation and Estimation

Contact states can be easily parameterized by the geometric properties of the manipulated object and its environment. As a simple example, consider a cylindrical object pivoting on a corner (Fig. 1.) In this example, the

location of the contact state can be parameterized by the position of the corner and the radius of the object.



FIG. 1. Example of one point contact state.

In this paper, we assume that the task decomposition problem has been solved and that there is a finite number of contact states that may be active. Each contact state can be expressed using sets of parameterized constraint equations that describe the motion of the contact state in different frames. For example, point contact between the manipulated object and an environment object can be expressed as

$$\begin{aligned} f_j(X_c^m(t), Y_c^m(t), Z_c^m(t)) &= 0 \\ g_j(X_c^e(t), Y_c^e(t), Z_c^e(t)) &= 0 \end{aligned} \quad (1)$$

Here, f_j and g_j are vector-valued functions of the j^{th} contact's coordinates written with respect to body frames of the manipulated object, (X_c^m, Y_c^m, Z_c^m) , and the environment object, (X_c^e, Y_c^e, Z_c^e) . These functions are related through the kinematic closure equation

$$T_o^m(t) \begin{bmatrix} X_c(t) \\ Y_c(t) \\ Z_c(t) \\ 1 \end{bmatrix}^m = T_o^e(t) \begin{bmatrix} X_c(t) \\ Y_c(t) \\ Z_c(t) \\ 1 \end{bmatrix}^e \quad (2)$$

in which $T_o^m(t)$ is a homogeneous transform matrix which relates the manipulated object body frame, through the remote manipulator's kinematics, to the remote environment base frame. Similarly, $T_o^e(t)$ relates the environment object body frame to the remote environment base frame. At any instant, these transform matrices are identical for all active constraints pairs of the form given by (1).

While it is assumed that the remote manipulator's configuration is known, $T_o^m(t)$ also depends on the possibly unknown grasp configuration of the manipulated object, leading to additional unknowns in $T_o^m(t)$. In addition, the base frame location of the environment object may be unknown leading to additional free parameters in $T_o^e(t)$. If the environment object or the object is not moving or deforming in its associated frame, then matrices T_o^e and T_o^m are time independent.

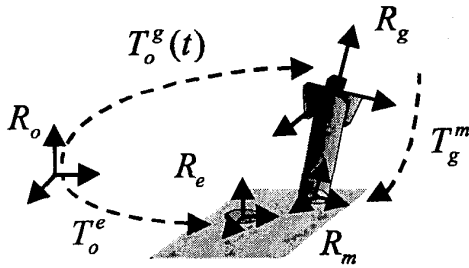


FIG. 2. Kinematic closure equation.

In order to create and solve an overdetermined problem, a minimal number of constraint equations are necessary at each time step. In n time steps, the kinematic closure equations (2) introduce $3n$ equations with $6n + v$ unknowns. Assuming that the constraint equations will also introduce a finite number η of unknown parameters, the number k of constraint equations must satisfy

$$kn > 3n + \eta + v \quad (3)$$

Thus, at each time step, four independent constraint equations are needed to solve (2).

3.1. Anticipated Motion Constraints

While four constraint equations are needed for point-contact problems in three dimensions, the contact geometry may provide a lesser number. In these situations, additional constraints could be obtained either by adding sensors or by imposing restrictions on the estimable motion trajectories. The latter approach will be taken here.

The crucial point is that we do not force the operator to follow constrained trajectories. Instead, we select 'anticipated' motions that the operator is likely to produce at some point during the task. Success of data segmentation and property estimation then depends on the operator producing those constrained motions for at least some short time interval during the associated contact states. Consider, for example, the contact depicted in Fig. 1. The geometry provides only three constraint equations – one restricting the contact point to the cylinder's surface and two limiting the contact point to the intersection of two planes. During this contact state, it is likely that the operator may slide the peg across or along the edge for at least a short distance without rotating the cylinder about its axis. With the inclusion of such a constraint, this contact becomes well defined for estimation purposes.

3.2. Property Estimation

Equations (1) and (2) introduce time dependent and independent unknowns. If the contacting objects are

rigid solids and the environment changes only due to manipulation, the properties that we want to identify are time independent.

In order to solve for the desired parameters we first need to eliminate the time dependent unknowns by substituting (1) into (2). This step assumes that the set of constraint equations has been chosen such that it allows this substitution. Often, the resulting set of equations can be arranged as an overdetermined set of linear equations $Ax = b$, where b ($n \times 1$) and A ($n \times m$) are, respectively, the observation vector and the data matrix. A and b both depend on measurements through the components of $T_o^g(t)$. It is well known that an ill-conditioned data matrix will lead to poor estimates. To avoid this problem, sufficiently exciting trajectories are necessary as well as carefully selected parameterizations.

3.3. Data Segmentation

Segmentation is based on a multiple model estimation approach (Fig. 3.). First, each contact state is expressed as a set of equations parameterized by the desired properties. Then, total least squares is used inside a moving data window of fixed length to simultaneously estimate the properties associated with each contact model.

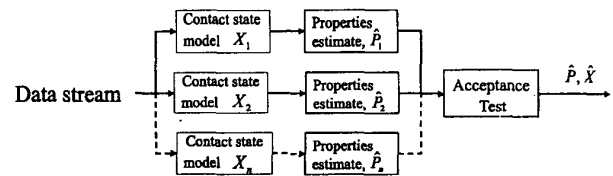


FIG. 3. Multiple model acceptance test.

To decide which contacts are active at each time step, an acceptance test is employed that compares the multiple correlation coefficients associated with each possible contact. This coefficient, defined by R^2 in (4), represents the proportion of variation in the vector b that can be explained by changes in the model. The closer R^2 is to one, the better the model accounts for the data. Ideally, we want all the variation to be explained.

$$R^2 = \frac{\text{explained variation}}{\text{total variation}} = \frac{\sum (\hat{b} - \bar{b})^2}{\sum (b - \bar{b})^2} \quad (4)$$

In order to test if a contact is active a threshold for R^2 must be selected. As a complement to the correlation coefficient, condition number is used to eliminate poorly excited trajectories. Task history and contact incompatibility, as embodied in the assumed task network of contact states, are also used to decide contact activity.

4. Experiment: 3D Peg-in-Hole Insertion

A tabletop teleoperator system composed of two PHAN-ToM® haptic devices is used to perform a spatial peg-in-hole insertion task. The desired outputs of the problem are the peg length and diameter, and the hole location and its diameter. The inputs consist of the remote manipulator joint angles. Constraint equations for the primary contacts, to be defined below, are also assumed known. A sketch of the system is shown in Fig. 4. Each device is a 6 degree of freedom manipulator. In order to accomplish the desired task, a gripper is added to the remote manipulator. The operator controls the master by manipulating a stylus attached through a passive spherical wrist.

At each sample time, the forward kinematics is computed such that the position and orientation of the end effector with respect to the base frame is known. The workspace is roughly a box of dimension 19.5 cm × 27 cm × 37.5 cm. Each device can exert a continuous tip force of 1.7 N, and a maximum force of 8.5 N can be achieved.

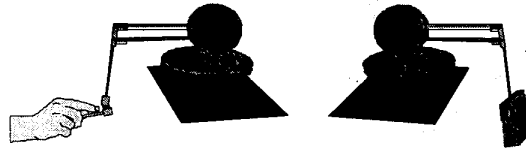


FIG. 4. Two PHANToM® haptic devices used as a teleoperator system.

The controller uses a symmetric proportional control scheme as described in [3]. The control loop rate is approximately 10 kHz.

4.1. Contact Constraints

In spatial peg-in-hole insertion, a limited number of one-point contacts can exist. Due to the symmetry of the peg and hole, four primary contacts can be defined as depicted in Fig. 5.

In Contact 1, for example, the contact point belongs to the bottom rim of the peg in R_m and to a plane in R_c .

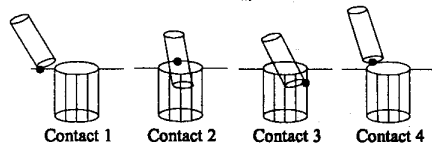


FIG. 5. One point contact states.

The primary contacts can each be described using equation (1). In addition to these simple contacts, surface and combined one point contacts can occur. Since parameterizations of the primary contacts can be selected to

include all of the desired geometric properties, only these contacts will be considered further. The sets of constraint equations for the primary contacts appear in (5)-(8).

<p><i>Contact 1</i></p> $Z_c^m(t) = 0$ <p>(5) $X_c^m(t)^2 + Y_c^m(t)^2 = R_{peg}^2$</p> $Z_c^e(t) = 0$	<p><i>Contact 2</i></p> $Z_c^e(t) = 0$ <p>(6) $X_c^m(t)^2 + Y_c^m(t)^2 = R_{peg}^2$</p> $X_c^e(t)^2 + Y_c^e(t)^2 = R_{hole}^2$
<p><i>Contact 3</i></p> $Z_c^m(t) = 0$ <p>(7) $X_c^m(t)^2 + Y_c^m(t)^2 = R_{peg}^2$</p> $X_c^e(t)^2 + Y_c^e(t)^2 = R_{hole}^2$	<p><i>Contact 4</i></p> $Z_c^m(t) = 0$ <p>(8) $X_c^m(t)^2 + Y_c^m(t)^2 = R_{peg}^2$</p> $Z_c^e(t) = 0$ $X_c^e(t)^2 + Y_c^e(t)^2 = R_{hole}^2$

4.2. Anticipated Motion Constraints

The geometry of the primary contacts as described by (5)-(8) provides three constraint equations for Contacts 1-3 and four for Contact 4. Since a minimum of four constraints are needed for estimation, the approach described in section 3.1 is employed to generate additional equations for Contacts 1-3. These constraints are based on motions the operator is likely to employ during the assembly task. The following list describes the constrained motions selected for this example. While the choice of motion constraints is not unique, those described here have been found to be well suited to the task.

- *Contact 1* – The peg slides on a plane in R_c without rotating about its axis. Thus, the contact point is fixed in R_m introducing one new constraint equation.
- *Contact 2* – The peg slides, without rotating about its axis, across a fixed point on the rim of the hole. Thus, the contact point is fixed in R_c and describes a line in R_m introducing two new equations.
- *Contact 3* – The peg slides, without rotating about its axis, along the cylindrical interior of the hole, parallel to the hole's axis. Thus, the contact point is fixed in R_m and describes a line R_c introducing two new constraint equations.

4.3. Constraint Simplification

A major difference between planar and spatial peg-in-hole insertion is the introduction of nonlinear constraint equations. These equations cause a problem when we want to insert (1) into (2) in order to obtain a set of linear equations. To avoid this problem, cylindrical coordinates are used to describe the position of the

contact point in the object frame. As an example, the mathematical description of Contact 1 is given assuming the contact point is fixed on the peg.

$$\begin{aligned} Z_c^m(t) &= 0 & X_c^m(t) &= R_{peg} \cos(\alpha) \\ Z_c^e(t) &= 0 & Y_c^m(t) &= R_{peg} \sin(\alpha) \\ \alpha &= \text{constant} & X_c^m(t)^2 + Y_c^m(t)^2 &= R_{peg}^2 \end{aligned} \quad (9)$$

To perform the desired task, the axis of the peg and hole must be aligned in space. In our formalism, position and orientation of both axes are given by the transformation matrices T_o^e and T_g^m . Each matrix is composed of a three by three rotation submatrix describing the orientation of the object and a three by one vector describing its position. The twelve components of each matrix are functions of only six independent parameters. Among these six parameters, only four are necessary to describe an axis in space, the remaining constants represent the length of the object or the vertical offset of the hole.

The following assumptions are made:

1. $T_o^e(t)$ is known.
2. T_o^e and T_g^m are time independent.
3. The grasping configuration of the object is known.
4. The orientation of the hole is known.

With these assumptions, the kinematic closure equations reduce to the following set of equations:

$$\underbrace{\begin{bmatrix} a_1(t) & a_2(t) & a_3(t) & a_4(t) \\ a_5(t) & a_6(t) & a_7(t) & a_8(t) \\ a_9(t) & a_{10}(t) & a_{11}(t) & a_{12}(t) \\ 0 & 0 & 0 & 1 \end{bmatrix}}_{T_o^e(t)} \underbrace{\begin{bmatrix} 1 & 0 & 0 & 0 \\ 0 & 1 & 0 & 0 \\ 0 & 0 & 1 & L_{peg} \\ 0 & 0 & 0 & 1 \end{bmatrix}}_{T_g^m} \underbrace{\begin{bmatrix} X_c(t) \\ Y_c(t) \\ Z_c(t) \\ 1 \end{bmatrix}}_{T_g^e} = \begin{bmatrix} 1 & 0 & 0 & T_z \\ 0 & 1 & 0 & T_y \\ 0 & 0 & 1 & T_x \\ 0 & 0 & 0 & 1 \end{bmatrix} \begin{bmatrix} X_o(t) \\ Y_o(t) \\ Z_o(t) \\ 1 \end{bmatrix} \quad (10)$$

T_g^m and T_o^e are created using, respectively, assumptions 2,3 and 4. Equation (10) can be reformulated as follows.

$$\begin{aligned} X_c^e(t) + T_x &= a_{11}(t)X_c^m(t) + a_{12}(t)Y_c^m(t) + a_{13}(t)(Z_c^m(t) + L_{peg}) + a_{14}(t) \\ Y_c^e(t) + T_y &= a_{21}(t)X_c^m(t) + a_{22}(t)Y_c^m(t) + a_{23}(t)(Z_c^m(t) + L_{peg}) + a_{24}(t) \\ Z_c^e(t) + T_z &= a_{31}(t)X_c^m(t) + a_{32}(t)Y_c^m(t) + a_{33}(t)(Z_c^m(t) + L_{peg}) + a_{34}(t) \end{aligned} \quad (11)$$

Finally, the constraint equations (5-8) are modified using the technique leading to (9) and inserted into (11).

For each contact state, the results lead to a set of overdetermined set of linear equations, $b = Ax$. For contacts 1, 2 and 3 of Fig. 5, these equations are given by (12), (13)

and (14), respectively. Contact 4 is not likely to occur during an insertion, and as a result, it is not considered.

$$a_{34} = [1 \quad -(a_{31} \cos \alpha + a_{32} \sin \alpha) \quad -a_{33}] \begin{bmatrix} T_z \\ R_{peg} \\ L_{peg} \end{bmatrix} \quad (12)$$

$$\begin{bmatrix} a_{14} - \frac{a_{12}a_{34}}{a_{33}} \\ a_{24} - \frac{a_{22}a_{34}}{a_{33}} \end{bmatrix} = \begin{bmatrix} 1 & 0 & \cos \alpha (\frac{a_{23}a_{31}}{a_{33}} - a_{11}) + \sin \alpha (\frac{a_{23}a_{32}}{a_{33}} - a_{12}) & -\frac{a_{13}}{a_{33}} \\ 0 & 1 & \cos \alpha (\frac{a_{23}a_{31}}{a_{33}} - a_{21}) + \sin \alpha (\frac{a_{23}a_{32}}{a_{33}} - a_{22}) & -\frac{a_{23}}{a_{33}} \end{bmatrix} \begin{bmatrix} H_x \\ H_y \\ R_{peg} \\ T_z \end{bmatrix} \quad (13)$$

$$\begin{bmatrix} a_{14} \\ a_{24} \end{bmatrix} = \begin{bmatrix} 1 & 0 & -(a_{11} \cos \alpha + a_{12} \sin \alpha) & -a_{13} \\ 0 & 1 & -(a_{21} \cos \alpha + a_{22} \sin \alpha) & -a_{23} \end{bmatrix} \begin{bmatrix} H_x \\ H_y \\ R_{peg} \\ L_{peg} \end{bmatrix} \quad (14)$$

In these equations, a_{ij} , $(i, j) \in \{1, \dots, 4\}$ and α are known and are time dependent. R_{peg} , L_{peg} represent the radius and length of the peg while T_z is the vertical offset of the drilled surface. H_x , H_y are the coordinates of a point on the cylindrical hole in the fixed frame. The last two parameters are the ones in which we are particularly interested because they contain information on the hole's center (T_x, T_y) . However, one can see that these parameters cannot be identified without the others.

4.4. Estimation

From (12)-(14), notice first that Contact 1 allows us to identify all of the parameters except those associated with the hole's axis. Secondly, notice that some parameters can be estimated in more than one contact state. Due to issues of numerical conditioning, however, it is often true that the quality of the estimates can vary considerably between contact states. One strategy for obtaining the best estimates employs a two-pass process. During the first pass, the entire data stream is segmented by contact state. For those parameters tied to multiple contact states, the estimates associated with the best-conditioned contact state are selected. These estimates are then utilized in estimating the remaining parameters.

Before testing this strategy for a complete insertion task, we first want to investigate the quality of the estimates obtainable from (12)-(14). The results of five trials associated with Contact 1, (12), are shown in Fig. 6. The direct measurements are indicated by dashed lines. Notice that the estimated results agree well with the measured ones regardless of the position of the contact point on the peg.

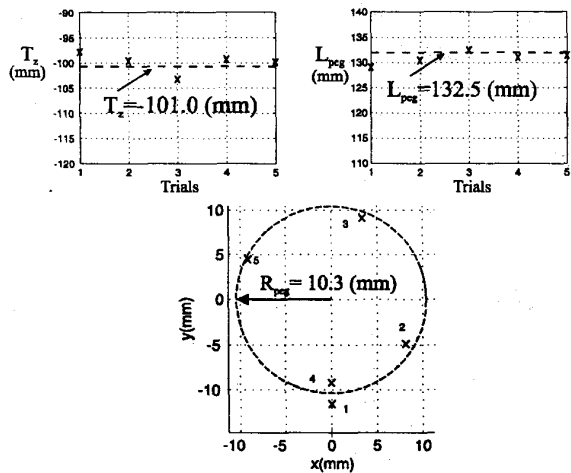


FIG. 6. Contact 1 estimates. T_z , L_{peg} and R_{peg} are the vertical offset of the hole, length and radius of the peg.

To test (13) and (14), three experimental trials of the double contact 2,3 were conducted. The estimates obtained from (12) are assumed known at this point and H_x, H_y are estimated. Points described by these two coordinates belong to the rim of the hole in the fixed frame. To obtain estimates of the hole's center and radius, a circle is fit through these points [7]. Fig. 7 shows the results for three different trials. Note that each of the two contacts yields its own estimate of H_x, H_y for each trial.

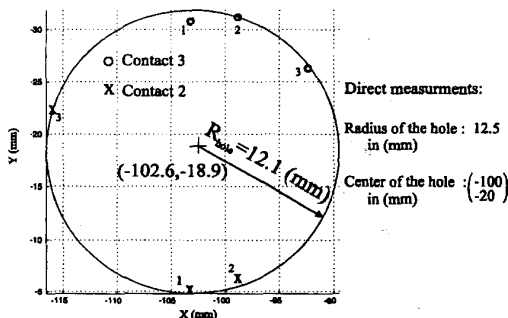


FIG. 7. Contact 2,3 estimates. Hole edge coordinates for three trials.

4.5. Segmentation and Estimation

The next series of results shows the automatic identification procedure applied to a spatial peg-in-hole insertion. As a mean of testing the automatic segmentation algorithm, the operator presses a switch during the task at each change of contact state. Orientation, position, and velocity of the robot's tip are recorded at a rate of 50Hz.

Fig. 8 depicts the anticipated sequence of contact states associated with the insertion task. First, the peg is slid toward the hole on the planar surface (Contact 1). As the peg enters the hole, it first pivots on the rim of the hole (Contact 2) and typically maintains this contact until the other side of the hole is reached. It then stays in double contact with the rim and the inside of the hole (Contacts 2,3) until the peg is inserted far enough that the task can be easily completed.

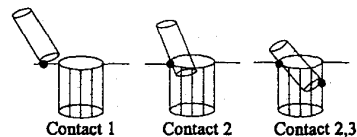


FIG. 8. Task decomposition function of the different contact states.

To estimate the desired peg and hole properties, it is necessary at a minimum to segment the data stream for these three contact states $\{1, 2, 2, 3\}$. Segmentation is performed using multiple model estimation on a 30-point moving data window. Contacts are accepted as active when $R^2 \geq 0.99$.

In Fig. 9, automatic segmentation is compared with manual segmentation as performed by the operator. Note that each contact has been correctly detected. For this experiment, the clearance ratio of the hole was chosen to be large to facilitate manual segmentation. Automatic segmentation of smaller clearance ratios has also been performed successfully.

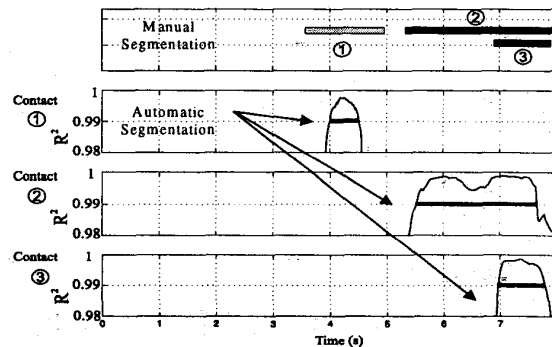


FIG. 9. Automatic versus manual segmentation.

For this set of contact states, Contact 1 is best conditioned for estimating T_z, L_{peg} and R_{peg} . These estimates are depicted in Fig. 10. They were obtained by averaging the parameters obtained by least squares for each data window within the segmented interval delineated by the two black dashed lines. (Note that least squares applied over the entire interval yielded comparable estimates.)

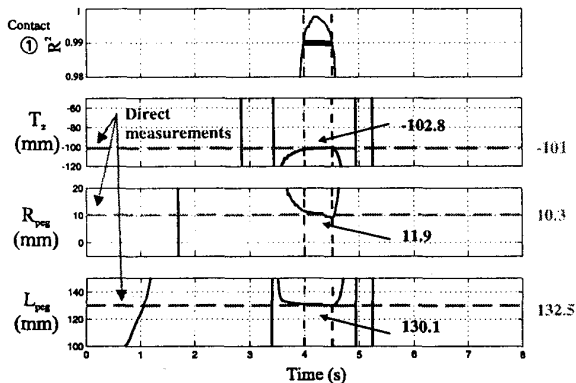


FIG. 10. Estimation of the properties T_z , L_{peg} , and R_{peg} associated with Contact 1.

Finally, the properties associated with Contacts 2,3 are estimated using the parameter values obtained from Contact 1. Equations (13) and (14) are used to find coordinates of points on the rim of the hole. A circle is fit through these points as shown in Fig. 11 to yield the hole's center coordinates and radius.

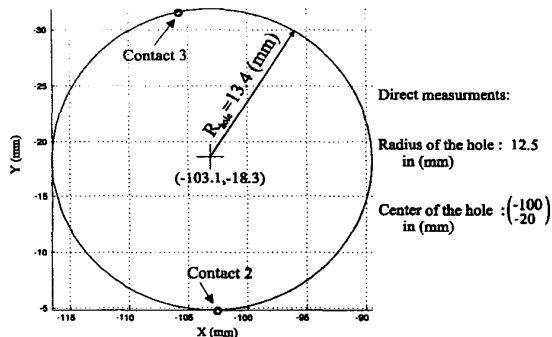


FIG. 11. Estimation of the hole's center and radius during Contact 2,3.

5. Conclusions

A simple method was presented for automatically estimating the geometric properties of manipulated objects and their environment during teleoperation. The approach relies on segmenting the kinematic data from the remote manipulator according to the active contacts between a manipulated object and its environment. A sufficient number of contact constraints for estimation were obtained by supplementing the geometric constraints with motion constraints based on anticipated motions of the operator. A tabletop teleoperator system was used to substantiate the approach.

While not pursued here, it is clear how such an approach could be extended to include both additional inputs (sensors) and outputs (object properties). Force data, for example, would allow the estimation of friction properties. For the peg insertion problem, the combination of geometric and friction properties would be sufficient to generate, using an assembly planner, on-line instructions for the operator so as to avoid jamming and wedging.

References

- [1] Bruyninckx, H., Dutré, S., and De Schutter, J. (1995). Peg-on-Hole: A Model Based Solution to Peg and Hole Alignment. *Proceedings of the 1995 IEEE Conference on Robotics and Automation*, 1919-1924.
- [2] Cai, C., and Roth, B. (1987). On the Spatial Motion of a Rigid Body with Point Contact. *Proceedings of the 1987 IEEE Conference on Robotics and Automation*, 686-695.
- [3] Debus, T., Dupont, P., and Howe, R. (1999). Automatic Property Identification via Parameterized Constraints. *Proceedings of the 1999 IEEE Conference on Robotics and Automation*, Detroit, MI, May.
- [4] Dupont, P., Schulteis, T., Millman, P and Howe, R. (1999). Automatic Identification of Environment Haptic Properties. *PRESENCE: Teleoperators and Virtual Environments*, 8(4), August, 392-409.
- [5] Eberman, B., and Salisbury, J. K. (1994). Application of change detection to dynamic contact sensing. *International Journal of Robotics Research*, (13)5, 369-394.
- [6] Fiorini, P., Losito, S., Giancaspro, A., and Pasquariello, G. (1992). Neural Networks for Off-line Segmentation of Teleoperation Tasks. *Proceedings of the 1992 IEEE International Symposium on Intelligent Control*, Glasgow, UK, 1, August, 17-22.
- [7] Gander, W., Golub, H. G., and Strebler, R. (1994). Least Squares Fitting of Circles and Ellipses. *BIT* (34), July, 558-578.
- [8] Griebenow, B.E. (1994). Buried-waste Integrated Demonstration Retrieval Projects. *Annual Meeting of American Nuclear Society*, New Orleans, LA, 19-23 June, *Trans. Am. Nucl. Soc.*, 70, 402.
- [9] Hannaford, B., and Lee, P. (1991). Hidden Markov Modal Analysis of Force/Torque Information in Telemanipulation. *International Journal of Robotics Research*, 10(5), October, 528-539.
- [10] Lin, S. T., and Yae, K. H. (1992). Identification of Unknown Payload and Environmental Parameters for Robot Compliant Motion. *Proceedings of the 1992 American Control Conference*, Chicago, 4, June, 2952-2956.
- [11] McCarragher, B. J., (1994a), Force Sensing from Human Demonstration Using a Hybrid Dynamical Model and Qualitative Reasoning. *Proceedings of the 1994 IEEE Conference on Robotics and Automation*, 1, May, 557-563.
- [12] McCarragher, B. J., (1994b). Petri Net Modeling for Robotic Assembly and Trajectory Planning. *IEEE Transactions on Industrial Electronics*, 41(6), December, 631-640.